Decrease in electrical contact resistance of Sb-doped n^+-$BaSi_2$ layers and spectral response of an Sb-doped n^+-$BaSi_2$/undoped $BaSi_2$ structure for solar cells

Komomo Kodama, Ryota Takabe, Suguru Yachi, Kaoru Toko, Takashi Suemasu*

Institute of Applied Physics, Graduate School of Pure and Applied Sciences, University of Tsukuba, Tsukuba, Ibaraki 305-8573, Japan

We investigated how the electron concentration n in a 300-nm-thick Sb-doped n^+-$BaSi_2$ layer grown by molecular beam epitaxy affected the contact resistance R_C to surface electrodes (Al, indium-tin-oxide). As the n of n-$BaSi_2$ increased, R_C decreased and reached a minimum of 0.019 Ω cm^2 at $n = 2.4 \times 10^{18}$ cm^{-3} for the Al electrodes. This value was more than one order of magnitude smaller than that obtained for Al/B-doped p-$BaSi_2$. We believe that this significant decrease in R_C came from Sb segregation. Furthermore, the internal quantum efficiency (*IQE*) spectrum was evaluated for an Sb-doped n^+-$BaSi_2$(20 nm)/undoped $BaSi_2$(500 nm)/n^+-Si(111) structure. Its *IQE* reached as high as ~50% over a wide wavelength range under a small bias voltage of 0.1 V applied between the top and bottom electrodes.

Email: suemasu@bk.tsukuba.ac.jp

1. Introduction

In many studies, various solar cells materials such as CdTe, chalcopyrites, kesterite, and perovskite have been assessed because of their low cost and high efficiency [1-6]. However, these materials contain elements that are scarce, toxic, or both. Thin-film Si solar cells have also been studied extensively; however, it is not easy to achieve efficiencies as high as 20% [7-17]. Thus, it is important to explore other materials for thin-film solar cells. Among such materials, we have focused on barium disilicide ($BaSi_2$), a semiconductor consisting of only abundant elements [18,19]. $BaSi_2$ is attractive for use in thin-film solar cells because of its bandgap of 1.3 eV, a matching solar spectrum [20], a high absorption coefficient of 3×10^4 cm^{-1} at 1.5 eV comparable to those of chalcopyrites [21-23], and superior minority-carrier diffusion length (L ~ 10 μm) [24,25] and lifetime (τ ~ 10 μs) [26-29]. Because of these properties, an energy conversion efficiency η of over 25% can be expected for a 2-μm-thick $BaSi_2$ pn-junction diode [30]. Recently, we have achieved a conversion efficiency near 10% with B-doped p-$BaSi_2$/n-Si heterojunction solar cells [31].

To fabricate $BaSi_2$ homojunction solar cells, we plan to use undoped $BaSi_2$ as an absorber layer in a solar cell. Undoped $BaSi_2$ has both a high α and a large L, both of which facilitate the collection of photogenerated carriers in an external circuit even though L degrades somewhat because of extrinsic effects such as crystal imperfections. In a solar cell, the topmost layer should be a heavily impurity-doped n- or p-type layer to decrease the contact resistance R_C, which directly affects the fill factor FF of the solar cell. As R_C increases, FF decreases and thus η decreases. In many studies, R_C have been assessed in solar cell materials [32-38]. In our previous work, we investigated the R_C between Al electrodes and B-doped p-$BaSi_2$. The R_C reached a minimum of 0.35 Ω cm^2 [31] when the hole concentration p of p-$BaSi_2$ was 4.0×10^{18} cm^{-3}. In this study, we first investigated the dependence of R_C between surface electrodes (Al or ITO) and Sb-doped n-$BaSi_2$ layers at various electron concentrations. We then evaluated the spectral response of an Sb-doped n^+-$BaSi_2$(20 nm)/undoped $BaSi_2$(500 nm) structure to verify how the heavily doped n^+-$BaSi_2$ surface layer affected the spectral response, especially at short wavelengths.

2. Experimental methods

Here, we used an ion-pumped molecular beam epitaxy (MBE) system equipped with an electron-beam evaporation source for Si as well as standard Knudsen cells for Ba and Sb. Details of the growth procedure of undoped $BaSi_2$ and Sb-doped n-$BaSi_2$ were reported previously [39,40]. To measure R_C, we used high-resistivity Czochralski (CZ) p-Si(111) substrates (resistivity ρ = 1000–10000 Ω cm) to minimize current flowing through the substrate. After thermally cleaning the substrate at the substrate temperature T_S = 900 °C, we deposited Ba at 500 °C to form an approximately 5-nm-thick $BaSi_2$ template layer by reactive deposition epitaxy. This template worked as seeds that control the crystal orientation of the $BaSi_2$ overlayers [41]. Next, we formed 300-nm-thick Sb-doped n-$BaSi_2$ epitaxial layers by MBE at various T_S values of 460 (sample A), 480 (sample B), 500 (sample C), and 520 °C (sample D). The electron concentration n of Sb-doped n-$BaSi_2$ depends on T_S [40]. Then, a 3-nm-thick a-Si passivation layer was deposited *in situ* at T_S = 180 °C [42]. Finally, 150-nm-thick striped Al or ITO electrodes (length l = 0.6 mm, width W = 7.0 mm, electrode interval d = 1.0 mm) were formed by sputtering. Carrier concentration was measured by the van der Pauw method at room temperature (RT). R_C was measured by the transfer length method at RT [43]. We compared the smallest R_C, $R_C = 0.35\ \Omega\ \mathrm{cm}^2$, measured from Al/p-$BaSi_2$ ($p = 4.0 \times 10^{18}\ \mathrm{cm}^{-3}$, sample E) [31]. The depth profile of Sb atoms was measured by secondary ion mass spectrometry (SIMS) using C_S^+ ions.

Next, we investigated the photoresponse properties of the Sb-doped n^+-$BaSi_2$/undoped $BaSi_2$ structure (sample F). A 500-nm-thick undoped $BaSi_2$ layer was epitaxially grown on a low-resistivity Cz n-Si(111) substrate ($\rho < 0.01$ Ω cm) at T_S = 580 °C, followed by a 20-nm-thick Sb-doped n$^+$-BaSi$_2$ ($n = 2.4 \times 10^{18}$ cm^{-3}) layer and a 3-nm-thick a-Si passivation layer. We used the low-resistivity Si substrate to exclude the contribution of photogenerated carriers in the n-Si substrate and to form a good electrical contact at the BaSi$_2$/Si heterointerface. Finally, 80-nm-thick ITO electrodes with a diameter of 1 mm and 150-nm-thick Al rear electrodes were formed by sputtering. The reflectance R and external quantum efficiency (EQE) spectra were evaluated at RT using a lock-in technique with a xenon lamp and a single monochromator (Bunko Keiki, SM-1700A and RU-60N) with a focal length of 25 cm. Internal quantum efficiency (IQE) was obtained by dividing the EQE by ($1-R$). Light intensity was calibrated using a pyroelectric sensor (Melles Griot, 13PEM001/J). The crystalline quality of the grown layers was characterized by reflection high-energy electron diffraction (RHEED) and X-ray diffraction (XRD) analyses using Cu Kα radiation.

3. Results and discussion

Figure 1 shows the θ–2θ XRD and RHEED patterns of samples A, B, C, and D. The RHEED patterns were observed along the Si $[11\bar{2}]$ azimuth. The diffraction peaks appeared only from the (100)-oriented BaSi$_2$ planes, such as (200), (400), and (600), showing that a-axis-oriented BaSi$_2$ epitaxial films were formed. However, the RHEED patterns were not streaky but spotty, meaning that the surface is rough. This surface roughness developed because the T_S for Sb-doped BaSi$_2$ was much lower [40] than the optimum T_S (~600 °C) for the undoped BaSi$_2$ absorber layers. The n values of samples A, B, C, and D were 6.9×10^{17}, 1.8×10^{18}, 2.4×10^{18}, and 2.8×10^{17} cm^{-3}, respectively. Now, using sample C as an example, we will show how to obtain R_C. Figure 2 shows the relationship between the measured resistance $r(x)$ between the Al or ITO electrodes and the electrode distance x for sample C ($n = 2.4 \times 10^{18}$ cm^{-3}, μ = 100 cm^2/V s). Ignoring the lateral resistance of the electrode when the current flows in the x direction,

$r(x)$ can be written as

$$r(x) \approx 2r_c + r_{\text{semi}}(x), \quad (1)$$

where $r_{\text{semi}}(x)$ is the resistance of the semiconductor and $2r_C$ is the intercept of the vertical axis when we plot $r(x)$ with respect to x. Because the second term on the right side of Eq. (1) is proportional to x, $r(x)$ increases with increasing x. As shown in Fig. 2, the line for the ITO electrodes has a slightly higher slope and thus a larger resistance than that for Al electrodes. This behavior probably occurred because the ITO electrode had larger lateral resistance than Al. From the plots in Fig. 2, r_c = 2.26 and 1.22 Ω were obtained for the ITO and Al electrodes, respectively. R_C is given by

$$R_C = r_c \times W \times L_t, \quad (2)$$

where L_t is the transfer length, which is half of the intercept of the horizontal axis of the straight line in Fig. 2. From Eq. (2), R_c was calculated to be 0.057 and 0.019 Ω cm^2 for the ITO and Al electrodes, respectively, in sample C.

Figure 3 summarizes the dependence of R_C on n for all the samples obtained by the method described above. R_C decreased with increasing n. The smallest R_C, 0.019 Ω·cm^2, was obtained from Al electrodes in sample C. This value is more than one order of magnitude smaller than the smallest R_C (0.35 Ω cm^2) obtained from Al/B-doped p-$BaSi_2$ ($p = 4.0 \times 10^{18}$ cm^{-3}, $\mu = 28$ $cm^2V^{-1}s^{-1}$) [31]. We will now discuss the reason for this behavior. According to Ref. 36, the sheet resistance R_{sheet} is given by

$$R_{\text{sheet}} = R_C / L_t^2 \,. \quad (2)$$

For sample C, R_{sheet} is 0.40 Ω from L_t = 0.218 mm and R_C = 0.019 Ω cm^2, while R_{sheet} equals 6.79 Ω using L_t = 0.227 mm and R_C = 0.35 Ω·cm^2 for sample E. Such a large difference in R_{sheet} between samples C and E cannot be anticipated from their similar ρ values: 0.0644 and 0.0557 Ω cm, respectively, which were determined by Hall measurements. It is known that B atoms in B-doped p-$BaSi_2$ do not segregate and so are almost uniformly distributed [44]. Figure 4 shows the depth profile of Sb atoms and secondary ions (Ba + Si) in sample C. The Sb atoms segregate toward the surface of sample C, and the Sb concentration exceeds 10^{20} cm^{-3} near the electrode. Segregation of Sb has been observed in various semiconductors such as Si, Ge, and III–V semiconductors [45-52]. Hence, n is actually much higher in the surface region than the n found from the Hall measurement ($n = 2.4 \times 10^{18}$ cm^{-3}), leading to the significant decrease in R_{sheet} and thus R_{C} in sample C. Owing to the segregation of Sb in $\mathrm{BaSi_2}$, an Sb-doped $\mathrm{n^+}$-$\mathrm{BaSi_2}$ layer should be placed on the top of the $\mathrm{BaSi_2}$ solar cell. Hence, an Sb-doped $\mathrm{n^+}$-$\mathrm{BaSi_2}$/undoped $\mathrm{BaSi_2}$ absorber layered structure is useful for practical applications.

We next assessed the spectral response of sample F, with an Sb-doped $\mathrm{n^+}$-$\mathrm{BaSi_2}$/undoped $\mathrm{BaSi_2}$ structure. Figure 5 shows a schematic of sample F for this purpose and the RHEED patterns obtained after the growth of each layer. Because $\mathrm{BaSi_2}$ has a large α, short-wavelength light is absorbed near the surface, in the Sb-doped $\mathrm{n^+}$-$\mathrm{BaSi_2}$ layer. Therefore, defective $\mathrm{n^+}$-$\mathrm{BaSi_2}$ deteriorates the solar-cell performance. Figure 6 shows the θ–2θ XRD pattern, revealing *a*-axis-oriented epitaxial growth up to the 20-nm-thick Sb-doped $\mathrm{n^+}$-$\mathrm{BaSi_2}$. Figure 7 shows the *IQE* spectrum of sample F. A bias voltage of –0.1 V was applied to the top ITO electrode with respect to the back side-surface Al electrode so that the photogenerated holes in the $\mathrm{BaSi_2}$ were extracted into the ITO electrode. The *IQE* increased sharply at wavelengths shorter than approximately 1000 nm, corresponding to the band gap of $\mathrm{BaSi_2}$, and reached approximately 50% over a wide wavelength range even under this small bias voltage. We observed no pronounced reduction in *IQE* at short wavelengths, even when a highly Sb-doped layer was inserted. In a $\mathrm{BaSi_2}$ homojunction solar cell, the built-in potential across the pn junction will be much higher than 0.1 V, producing larger *IQE*s. On the basis of these findings, we conclude that the Sb-doped $\mathrm{n^+}$-$\mathrm{BaSi_2}$/undoped $\mathrm{BaSi_2}$ absorber layered structure is suitable for practical $\mathrm{BaSi_2}$ solar cells.

4. Conclusions

We investigated the dependence of R_C on the electron concentration of Sb-doped n-$BaSi_2$ and achieved a minimum R_C of 0.019 Ω cm^2 for Al/Sb-doped n-$BaSi_2$ at $n = 2.4 \times 10^{18}$ cm^{-3}. This R_C was more than one order of magnitude smaller than the R_C obtained for Al/B-doped p-$BaSi_2$, 0.35 Ω·cm^2. We explained this significant reduction in R_C in Al/Sb-doped n-$BaSi_2$ as being due to Sb segregation, which was verified by SIMS. The concentration of Sb atoms exceeded 10^{20} cm^{-3} near the electrode, significantly decreasing R_C. We achieved an *IQE* > 50% over a wide wavelength range under a small bias voltage of 0.1 V in the n^+(20 nm)/undoped $BaSi_2$(500 nm)/n^+-Si(111) structure.

Acknowledgements

This work was financially supported by JSPS KAKENHI Grant Numbers 15H02237 and 17K18865. R.T. was financially supported by a Grant-in-Aid for JSPS Fellows (15J02139).

References

[1] M. G. Panthani, V. Akhavan, B. Goodfellow, J. P. Schmidtke, L. Dunn, A. Dodabalapur, P. F. Barbara, and B. A. Korgel, J. Am. Chem. Soc. **130**, 16770 (2008).

[2] W. Jaegermann, A. Klein, and T. Mayer, Adv. Mater. **21**, 4196 (2009).

[3] S. Ahmed, K. B. Reuter, O. Gunawan, L. Guo, L. T. Romankiw, and H. Deligianni, Adv. Energy Mater. **2**, 253 (2012).

[4] C. Steinhagen, M. G. Panthani, V. Akhavan, B. Goodfellow, B. Koo, and B. A. Korgel, J. Am. Chem. Soc. **131**, 12554 (2009).

[5] M. A. Green, A. Ho-Baillie, and H. J. Snaith, Nat. Photonics **8**, 506 (2014).

[6] H. S. Kim, S. H. Im, and N. G. Park, J. Phys. Chem. C **118**, 5615 (2014).

[7] R. G. Gordon, J. Proscia, F. B. Ellis, Jr., and A. E. Delahoy, Sol. Energy Mater. **18**, 263 (1989).

[8] P. Campbell, Sol. Energy Mater. **21**, 165 (1990).

[9] H. Sasaki, H. Morikawa, Y. Matsuno, M. Deguchi, T. Ishihara, H. Kumabe, T. Murotani, and S. Mitsui, Jpn. J. Appl. Phys. **33**, 3389 (1994).

[10] J. Meier, S. Dubail, R. Platz, P. Torres, U. Kroll, J. A. A. Selvan, N. P. Vaucher, Ch. Hof, D. Fischer, H. Keppner, R. Flückiger, A. Shah, V. Shklover, and K.-D. Ufert, Sol. Energy Mater. Sol. Cells **49**, 35 (1997).

[11] O. Vetterl, F. Finger, R. Carius, P. Hapke, L. Houben, O. Kluth, A. Lambertz, A. Mück, B. Rech, and H. Wagner, Sol. Energy Mater. Sol. Cells **62**, 97 (2000).

[12] A. Poruba, A. Fejfar, Z. Remes, J. Springer, M. Vanecek, and J. Kocka, J. Appl. Phys. **88**, 148 (2000).

[13] J. Müller, B. Rech, J. Springer, and M. Vanecek, Sol. Energy **77**, 917 (2004).

[14] M. Berginski, J. Hüpkes, M. Schulte, G. Schöpe, H. Stiebig, and B. Rech, J. Appl. Phys. **101**, 074903 (2007).

[15] D. Zhou and R. Biswas, J. Appl. Phys. **103**, 093102 (2008).

[16] A. Hongsingthong, T. Krajangsang, I. A. Yunaz, S. Miyajima, and M. Konagai, Appl. Phys. Express **3**, 051102 (2010).

[17] H. Sai, Y. Kanamori, and M. Kondo, Appl. Phys. Lett. **98**, 113502 (2011).

[18] J. Evers, G. Oehlinger, and A. Weiss, Angew. Chem., Int. Ed. **16**, 659 (1977).

[19] M. Imai and T. Hirano, J. Alloys Compd. **224**, 111 (1995).

[20] K. Morita, Y. Inomata, and T. Suemasu, Thin Solid Films **508**, 363 (2006).

[21] D. B. Migas, V. L. Shaposhnikov, and V. E. Borisenko, Phys. Status Solidi B **244**, 2611 (2007).

[22] K. Toh, T. Saito, and T. Suemasu, Jpn. J. Appl. Phys. **50**, 068001 (2011).

[23] M. Kumar, N. Umezawa, and M. Imai, J. Appl. Phys. **115**, 203718 (2014).

[24] M. Baba, K. Toh, K. Toko, N. Saito, N. Yoshizawa, K. Jiptner, T. Sakiguchi, K. O. Hara, N. Usami, and T. Suemasu, J. Cryst. Growth **348**, 75 (2012).

[25] M. Baba, K. Watanabe, K. O. Hara, K. Toko, T. Sekiguchi, N. Usami, and T. Suemasu, Jpn. J. Appl. Phys. **53**, 078004 (2014).

[26] K. O. Hara, N. Usami, K. Toh, M. Baba, T. Toko, and T. Suemasu, J. Appl. Phys. **112**, 083108 (2012).

[27] K. O. Hara, N. Usami, K. Nakamura, R. Takabe, M. Baba, K. Toko, and T. Suemasu, Appl. Phys. Express **6**, 112302 (2013).

[28] R. Takabe, K. O. Hara, M. Baba, W. Du, N. Shimada, K. Toko, N. Usami, and T. Suemasu, J. Appl. Phys. **115**, 193510 (2014).

[29] T. Suemasu and N. Usami, J. Phys. D Appl. Phys. **50**, 023001 (2017).

[30] T. Suemasu, Jpn. J. Appl. Phys. **54**, 07JA01 (2015).

[31] S. Yachi, R. Takabe, K.Toko, and T. Suemasu, Appl. Phys. Lett. **109**, 072103 (2016).

[32] D. K. Schroder and D. L. Meier, IEEE Trans. Electron Devices **31**, 637 (1984).

[33] S. Y. Lee, H. Choi, H. Li, K. Ji, S. Nam, J. Choi, S. W. Ahn, H. M. Lee, and B. Park, Sol. Energy Mater. Sol. Cells **120**, 412 (2014).

[34] G. J. Bauhuis, P. Mulder, E. J. Haverkamp, J. C. C. M. Hujiben, and J. J. Schermer, Sol. Energy Mater. Sol. Cells **93**, 1488 (2009).

[35] K. Kuribayashi, H. Matsumoto, H. Uda, Y. Komatsu, A. Nakano, and S. Ikegami, Jpn. J. Appl. Phys. **22**, 1828 (1983).

[36] K. Nishioka, T. Takamoto, T. Agui, M. Kaneiwa, Y. Uraoka, and T. Fuyuki, Sol. Energy Mater. Sol. Cells **90**, 1308 (2006).

[37] M. A. Khan, M. S. Shur, and Q. Chen, Appl. Phys. Lett. **68**, 3022 (1996).

[38] L. L. Smith, R. F. Davis, M. J. Kim, R. W. Carpenter, and Y. Huang, J. Master. Res. **12**, 2249 (1997).

[39] R. Takabe, K. Nakamura, M. Baba, W. Du, M. Ajmal Khan, K. Toko, M. Sasase, K. O. Hara, N. Usami, and T. Suemasu, Jpn. J. Appl. Phys. **53**, 04ER04 (2014).

[40] M. Kobayashi, Y. Matsumoto, Y. Ichikawa, D. Tsukada, and T. Suemasu, Appl. Phys. Express **1**, 051403 (2008).

[41] Y. Inomata, T. Nakamura, T. Suemasu, and F. Hasegawa, Jpn. J. Appl. Phys. **43**, L478 (2004).

[42] R. Takabe, H. Takeuchi, W. Du, K. Ito, K. Toko, S. Ueda, A. Kimura, and T. Suemasu, J. Appl. Phys. **119**, 165304 (2016).

[43] P. N. Vinod, J. Mater. Sci.: Mater. Electron. **22**, 1248 (2011).

[44] D. Tsukahara, M. Baba, K. Watanabe, T. Kimura, K. O. Hara, W. Du, N. Usami, K. Toko, T. Sekiguchi, and T. Sumasu, Jpn. J. Appl. Phys. **54**, 030306 (2015).

[45] K. D. Hobart, D. J. Godbey, M. E. Twigg, M. Fatemi, and P. E. Thompson, Surf. Sci. **334**, 29 (1995).

[46] A. Gulino, G. G. Condorelli, K. Fragala, and R. G. Egdell, Appl. Surf. Sci. **90**, 289 (1995).

Si

[47] R. Kaspi and K. R. Evans, J. Cryst. Growth **175**, 838 (1997).

[48] D. Reinking, M. Kammler, M. HornVonHoegen, and K. R. Hofmann, Appl. Phys. Lett. **71**, 924 (1997).

[49] O. J. Pitts, S. P. Watkins, C. X. Wang, V. Fink, and K. L. Kavanagh, J. Cryst. Growth **254**, 28 (2003).

[50] H. S. Wong, L. Chan, G. Sainudra, and Y. C. Yeo, IEEE Trans. Electron Devices **18**, 703 (2007).

[51] M. Oehme, J. Werner, and E. Kasper, J. Cryst. Growth **310**, 4531 (2008).

[52] D. V. Yurasov, A. V. Antonov, M. N. Drozdov, V. B. Schmagin, K. E. Spirin, and A. V. Novikov, J. Appl. Phys. **118**, 145701 (2015).

Figure captions

Fig. 1 θ–2θ XRD and RHEED patterns observed along the Si $[11\bar{2}]$ azimuth of samples A, B, C, and D. The asterisk (*) indicates the diffraction of the Si substrate used.

Fig. 2 Sample structure for R_C measurement and the relationships between resistance and Al or ITO electrode distance for sample C, Sb-doped n-$BaSi_2$ ($n = 2.4 \times 10^{18}$ cm^{-3}).

Fig. 3 R_C as a function of electron concentration for Al/n-$BaSi_2$ and ITO/n-$BaSi_2$. The smallest R_C (0.35 Ω cm^2) obtained from Al/p-$BaSi_2$ [31] is shown for comparison.

Fig. 4 SIMS depth profile of Sb atoms and secondary ions (Ba + Si).

Fig. 5 Sample structure of sample F and RHEED patterns of each layer observed along the Si $[1\bar{1}0]$ azimuth.

Fig. 6 θ–2θ XRD pattern of sample F. The asterisk (*) indicates the diffraction of the Si substrate used.

Fig. 7 *IQE* spectrum of sample F under a bias voltage of -0.1 V applied to the surface ITO electrode with respect to the back side-surface Al electrode.

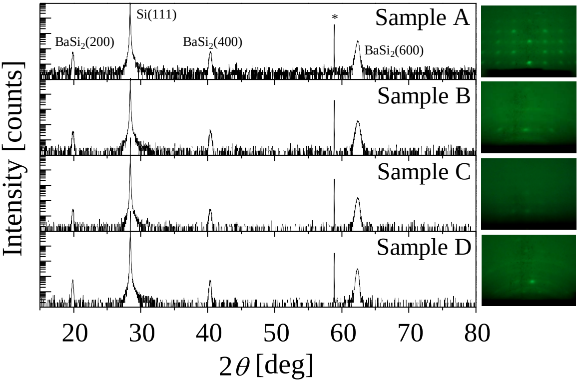
Intensity [counts]
Sample A
Sample B
Sample C
Sample D
Si(111)
*
$BaSi_2(200)$
$BaSi_2(400)$
$BaSi_2(600)$
20
30
40
50
60
70
80
2θ [deg]

Fig. 1

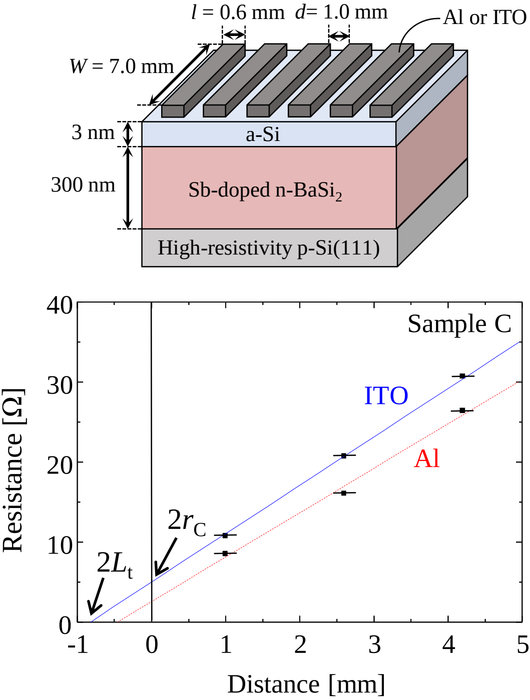
l = 0.6 mm
d= 1.0 mm
Al or ITO
W = 7.0 mm
3 nm
a-Si
300 nm
Sb-doped n-$BaSi_2$
High-resistivity p-Si(111)
Sample C
ITO
Al
$2r_C$
$2L_t$
Resistance [Ω]
0
10
20
30
40
-1
0
1
2
3
4
5
Distance [mm]

Fig. 2

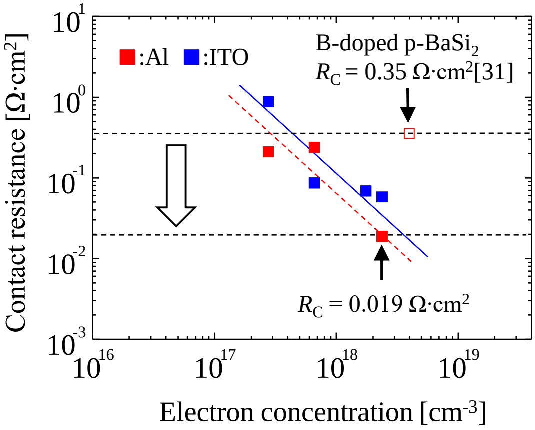

Contact resistance [Ω·cm²]
Electron concentration [cm⁻³]
10¹
10⁰
10⁻¹
10⁻²
10⁻³
10¹⁶
10¹⁷
10¹⁸
10¹⁹
■:Al ■:ITO
B-doped p-BaSi₂
R_C = 0.35 Ω·cm²[31]
R_C = 0.019 Ω·cm²

Fig. 3

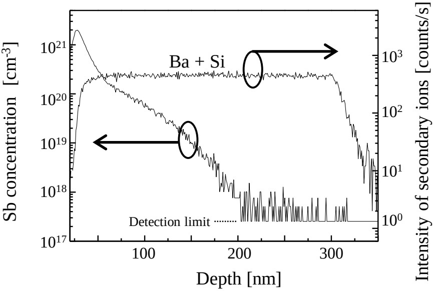

Sb concentration [cm-3]
10^{21}
10^{20}
10^{19}
10^{18}
10^{17}
Ba + Si
Detection limit
100
200
300
Depth [nm]
10^{3}
10^{2}
10^{1}
10^{0}
Intensity of secondary ions [counts/s]

Fig. 4

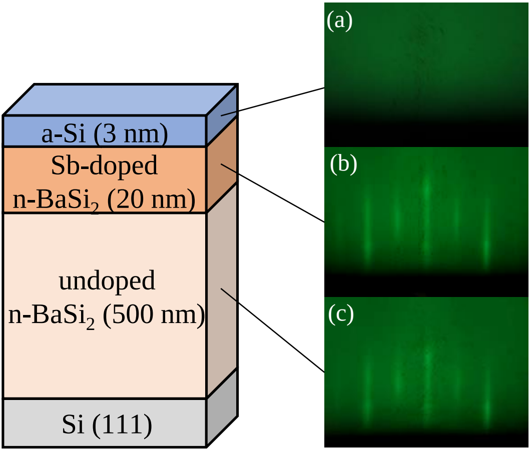

Fig. 5

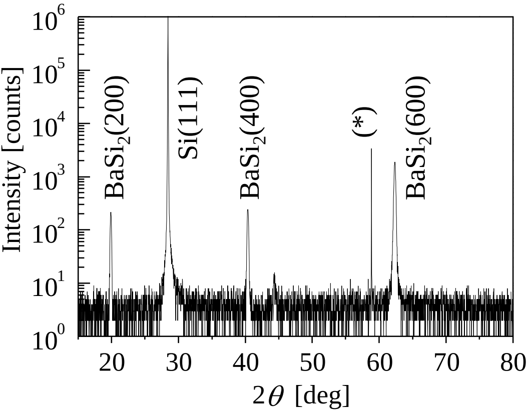
Intensity [counts]
10^0
10^1
10^2
10^3
10^4
10^5
10^6
$BaSi_2(200)$
Si(111)
$BaSi_2(400)$
(*)
$BaSi_2(600)$
20
30
40
50
60
70
80
2θ [deg]

Fig. 6

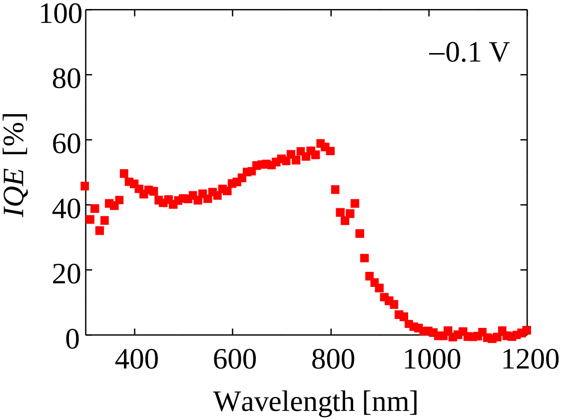

Fig. 7